

Projected Performance of a Cryogenic Particle Detector for a WIMP Dark Matter Search

Matthew D. Truch
with Prof. Daniel S. Akerib

May 1, 2000

Abstract

The Cryogenic Dark Matter Search (CDMS) collaboration detectors are designed to detect Weakly Interacting Massive Particles (WIMPs) by independently measuring deposited charge and phonon energy. Phonon energy measurement utilizes quasi-particle trap assisted electrothermal feedback Transition Edge Sensors (or QETs). The effects of variations in the steepness of the superconducting transition, α , and the transition temperature, T_c , are examined.

Test wafers of thin tungsten films are diced, and T_c and α measurements are made at several locations on a wafer. Trends in T_c and α are examined, and phonon energy resolution for a CDMS detector is plotted as a function of position on actual test wafers. Recent advances in sputtering techniques minimize T_c gradients while magnetic impurity implantation tunes T_c . Because of these changes, detector performance is expected to be better than before.

1 Introduction and Motivation

1.1 Evidence for Dark Matter

Recent estimates of the Hubble constant, H_0 , and precise measurements of the Cosmic Microwave Background (CMB) radiation has allowed the determination of many cosmological constants to unprecedented accuracy. However, careful study is required to understand the remaining problems. One of them is the dark matter problem.

The density of matter in the universe is often reported as its ratio to the critical density

$$\Omega \equiv \frac{\rho}{\rho_{\text{crit}}}$$

as

$$\Omega_M = \Omega_B + \Omega_{\text{missing}}.$$

Ω_B , is baryonic matter, and Ω_{missing} is non-baryonic matter. If $\Omega_M > \Omega_B$ than there must be non-baryonic matter that makes up the difference. [17]

The most important factor in determining the baryonic density is Big Bang Nucleosynthesis (BBN). BBN predicts a different primordial amount of each light nucleus for a given baryonic density. Because deuterium is not produced in any other cosmological process, measuring current deuterium abundance is our best probe of the primordial universe. Some high redshift (old) hydrogen clouds are backlit by QSOs. We can measure the hydrogen and deuterium lines in the cloud, to measure the ratio of hydrogen to deuterium. Current deuterium abundances measured with this technique give $\Omega_B h = 0.02 \pm .002$.¹ Independently, measuring the opacity of the lyman- α forest in high redshift quasars places a lower limit of $\Omega_B h > 0.015$. The two independent measurements agree.

Gravity affects all mass, baryonic and non-baryonic, so gravity is used to measure Ω_M . Rich clusters are very large, but rare astronomical objects. They are so large that we expect them to be a good sample of the universe, therefore measuring properties of a cluster is like measuring the properties of the universe. To measure Ω_M , we must assume that the following ratio holds:

$$\left(\frac{m_B}{m_{\text{total}}} \right)_{\text{cluster}} = \frac{\Omega_B}{\Omega_M}$$

The mass of the baryons in the cluster are measured from the intensity of the hot x-ray emitting gas and from the optical light from stars in galaxies contained within the cluster.

The total mass of the cluster is measured in 3 independent ways: using the techniques of gravitational lensing, assuming the gas is in hydrostatic equilibrium, or by measuring the motions of the cluster and applying the virial theorem (the dynamical mass).

The amount of baryonic matter in the cluster can be measured by investigating the hot, x-ray emitting hydrogen gas. This is because most of the baryons in the cluster are in the hot

¹ h is a dimensionless constant derived from the definition:

$$H_0 \equiv 100h \frac{\text{km}}{\text{s} \cdot \text{Mpc}}.$$

gases, and not in stars. Therefore the flux of photons from the hot gas will be proportional to the baryonic mass of the cluster.

Experimentally it is found that all methods for measuring the mass agree with each other, and indicate a total mass density of $\Omega_M = 0.4 \pm 0.1$.

Locally the dark matter problem is important too. Comparisons of actual galactic rotation curves and rotation curves consistent with the visible matter in our galaxy yield large discrepancies. If a spherical halo of dark matter is also present in the galaxy, and appropriate dark matter density will compensate for the observed rotation curves. [2, 5, 10] Current measurements suggest that in the halo of our galaxy, the density of dark matter is a few orders of magnitude larger than the average density in the universe.

This is the motivation for a dark matter search. From different independent and stable measuring techniques, we find that there is more matter in the universe than the baryons can account for. We must search for the missing matter, the dark matter.

1.2 Types of Dark Matter

If we need to search for this dark matter, we need to know what it is. The term *non-baryonic* means anything not made up of baryons, however in the terms of current theory, it is predicted to be a relic particle of the Big Bang. These relic particles can be categorized as hot, warm, or cold, indicating at which stage they “froze” out of the Big Bang.

If Γ_x is the reaction rate of particle x and H_0 is the Hubble constant, then

$$\frac{\Gamma}{H_0} \approx 1$$

is the freezeout condition for particle x. In other words, once the mean free time ($1/\Gamma_x$) is about equal to the age of the universe ($1/H_0$), the particle will no longer remain in equilibrium, preserving its number density at freezeout.

Dark matter has been classified into 3 main categories, hot, warm, and cold. ‘Hot’ or ‘cold’ refers to the temperature, or average random velocity, or a particle at freezeout.

Hot Dark Matter (HDM) decouples from the Big Bang while relativistic. It would have a number density on the order of that for photons. The prime example is the neutrino, as they have now been found to have finite mass. [15] However, although it can account for the missing mass, HDM does a poor job reproducing observed structure of the universe after extensive N-body simulations, and cannot explain the galactic halo (because of the Pauli exclusion principle). [10] For these reasons, HDM is not favored as a viable candidate.

Warm Dark Matter (WDM) is the least likely type of dark matter. It would have a mass on the order of $1 - 10\text{eV}$. [15]

Cold Dark Matter (CDM) is dark matter that decoupled from the Big Bang while non-relativistic. It has been shown that if CDM particles contribute most of the dark matter required to close the universe, $M_{\text{WIMP}} \geq 2\text{GeV}/c^2$. [11] In any case, the theoretically preferred range of masses is $10\text{GeV} < M_{\text{WIMP}} < 1000\text{GeV}$. WIMP is a general term, which refers to any particle with a large mass and which only interacts via the weak (and gravitational) forces. However, supersymmetry (SUSY) predicts a particle with WIMP-like properties which is often referred to as a WIMP, although not the exclusive form of WIMPs. [7]

1.3 WIMPs

Several SUSY theories predict that the lightest supersymmetric particle (LSP) is the best WIMP candidate. It would be a neutralino, a linear combination of the supersymmetric partners of the photon, Z^0 , and Higgs bosons. There is little certainty in the exact makeup of the LSP, as SUSY is a group of theories, which extend beyond the Standard Model, and have yet to be directly confirmed.

Although detailed parameters of WIMPs are unavailable from theory, some useful quantities can be calculated. Because WIMPs are non-relativistic at freezeout, one can use the number density of non-relativistic thermal particles equation in freezeout number density calculations:

$$n = g \left(\frac{mT}{2\pi} \right)^{3/2} e^{-m/T}.$$

Here g is the number of degrees of freedom, m is the mass, and T is the current temperature. From above, freezeout occurs when $\Gamma/H_0 \approx 1$, where $\Gamma = n \langle \sigma v \rangle$. From dimensional arguments, $\sigma \sim G_F^2 m^2$. This leads us to the freezeout condition [15]

$$\left(\frac{m}{2.2\text{MeV}} \right)^3 \sqrt{\frac{m}{T}} e^{-m/T} \sim 1.$$

If one assumes a WIMP mass of 40GeV, $n_{today} = 5 \times 10^{-3} \text{WIMPs/m}^2$, and the density, $\rho = 10^{-28} \text{kg/m}^3$. This value is on the order of what is required to close the universe, i.e. $\Omega_{\text{WIMP}} \sim 1$.

If these WIMPs make up the dark matter contained within the dark matter halo of our galaxy, several WIMPs will bombard the earth every second. It is usually assumed that the dark matter halo will be in a Maxwellian distribution, with $\langle v_{\text{WIMP}} \rangle = 220 \text{km/s}$. [12]

With an assumption about the cross section, σ , of WIMP-nucleus recoils and the above parameters, an event rate can be calculated for earth based detectors. The event rate, R , is given by

$$dR = \frac{N_0}{A} \sigma v_{\text{WIMP}} dn,$$

where N_0 is Avogadro's number, and A is the atomic mass of the target nucleus (in AMUs). In low background experiments, rates on the order of 1 event per kg of detector per day are not uncommon. [12, 6] This is a small, but workable rate. Earth based detectors could probe the dark matter, given they can have significant mass ($> 1\text{kg}$), are capable for running for a long period of time, and are capable of distinguishing WIMPs from background noise. WIMPs have a larger scattering cross section from nuclei than from electrons because WIMPs scatter coherently from quarks in the nuclei, but several charged particle background events will have a larger scattering cross section from electrons because of the electromagnetic force.

2 CDMS — The Experiment

The Cryogenic Dark Matter Search (CDMS) has been designed to meet the needs of an earth based dark matter search as outlined above. CDMS detectors are large ($\approx 250\text{g}$ per germanium crystal; several detectors can run at one time), are capable of running for extended

periods, and most important, are able to discern WIMPs from most other background events. Basics of CDMS are outlined in the following section, before an in-depth discussion of the phonon measurement, of which this thesis is based.

2.1 Background

The main background for CDMS detectors is energy deposition in the detectors that are *not* caused by a WIMP, but deposit energy in the same way as a WIMP. To keep the background low, the detectors are placed deep underground, shielded with lead and polyethylene, and all internal parts are made from radio-pure materials. A deep underground location is used to moderate high energy cosmic rays and muons. The lead is used to stop high energy γ s and x-rays, and the polyethylene moderates incoming neutrons, which are usually caused by high energy muons interacting in the nearby rock. Since WIMPs have a small cross section and rarely interact in the shield, the signal to background ratio is increased. Unfortunately this is not enough to bring the background rate below the expected WIMP rate, therefore an active veto is used to exclude events caused by charged particles, like muons.

The active veto is a plastic scintillator placed around the detector. If light is collected by photo multiplier tubes attached to the scintillator, any immediate event in the detector is ruled out, as only cosmic rays or other high energy γ s will trigger the veto and interact in the detector at the same time. There is a small chance that a WIMP will interact with the detector during this dead-time, and will be rejected. Estimates put this loss at a 10% reduction in WIMP events. [1]

The main advantage of CDMS detectors over other WIMP searches is their ability to measure charge and phonon energy deposited by an event. Because nuclear recoils deposit less charge energy per amount of phonon energy than electron recoils, measuring both allows simple discrimination between the two types of recoils. This is important because most background events recoil off the electrons in a detector, but WIMPs are electrically neutral and will recoil off the nucleus. The only background event that is electrically neutral is the neutron, which can be rejected by the veto (if it came from a muon), or by multiple scatters in detectors. Because the cross section for WIMPs is so low, interactions in more than one detector simultaneously suggest neutron events. [14] In addition, the number of multiple neutron scatters is statistically related to the number of single neutron scatters. Therefore the number of multiple scatters can be used to statistically subtract single neutron events. [1, 16]

2.2 Charge (Ionization) Measurement

CDMS detectors are fabricated with electrodes on either side of the germanium crystal. See Figure 1. When an incoming particle recoils inside the germanium crystal, electron-hole pairs are generated. The number of electron-hole pairs is directly proportional to the energy of the incoming particle, with different constants of proportionality for different incident particles. The electrodes set up an electric field inside the detector, and the electron-hole pairs separate and drift to opposite electrodes. These charges are collected and amplified by

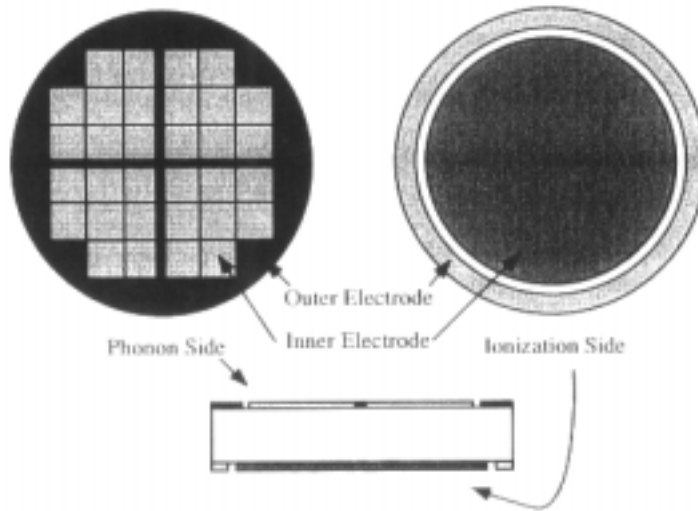


Figure 1: Top, bottom, and side view of a CDMS germanium detector indicating charge electrodes. The small squares on the phonon side contain several tungsten meanders each.

a charge-amp circuit (see figure 2) and recorded in the data acquisition computer, where the incident energy can be calculated.

2.3 Phonon Measurement

Phonons are collected in a different manner than ionization energy. When an incident particle interacts in the germanium crystal, phonons, or quantum lattice vibrations, are produced. At first, these phonons are athermal, i.e. at an energy above the temperature of the system, and are able to break cooper pairs. Athermal phonons will scatter off the surfaces of the germanium crystal until either they thermalize (and heat up the lattice) or are collected in quasi-particle traps placed on the surface of the germanium. The quasi-particle traps are made out of aluminium, which superconducts at the temperatures of our detectors. Quasi-particle traps are used to make more of the detector surface active. This could not be accomplished with tungsten, as tungsten's high heat capacity requires as little tungsten as possible in the sensor. [3] See figure 3 The tungsten meanders are set up as superconducting transition edge sensors (TES), and can accurately measure the amount of energy (heat) deposited in the tungsten.

A TES is biased in the middle of its superconducting transition, so a small change in temperature causes a large change in the resistance of the sensor. The TES used in CDMS detectors are set up in electrothermal feedback (ETF) mode: the tungsten is voltage biased, and joule heating causes the tungsten to heat above the substrate (crystal) temperature. Once the tungsten is at its superconducting transition temperature, T_c , its resistance in-

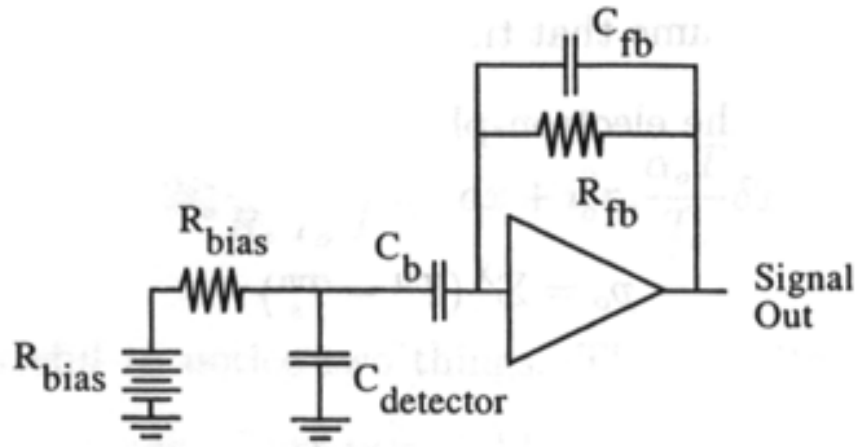


Figure 2: Simplified schematic of the CDMS charge circuit.

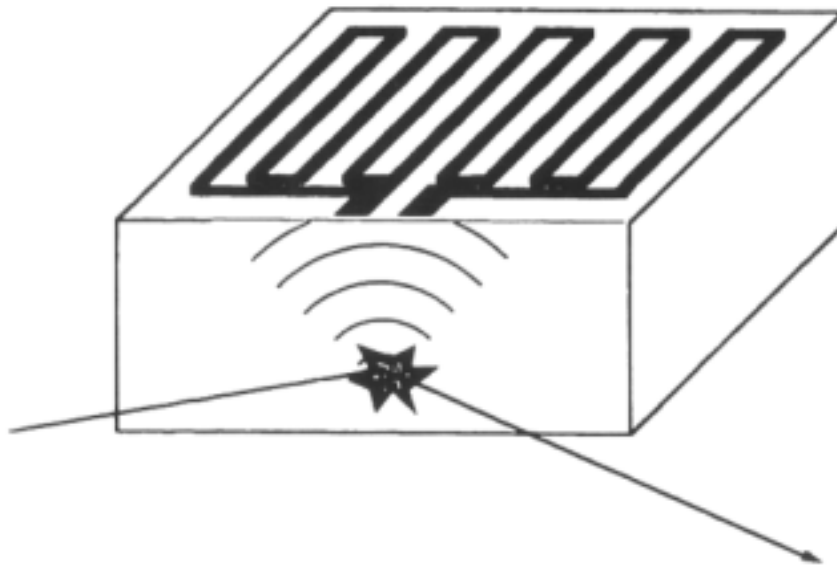


Figure 3: A simple drawing of a tungsten meander on a germanium detector. The incoming particle recoils off a germanium nucleus, phonons propagate to the meander, and eventually heat it up.

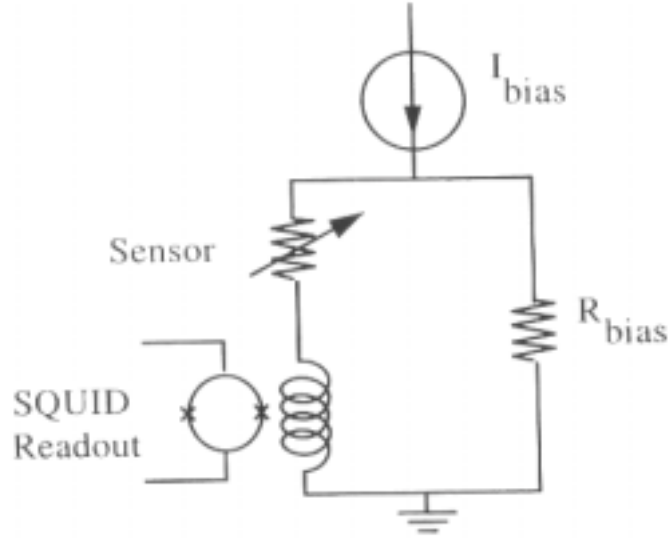


Figure 4: Simplified schematic of the CDMS SQUID readout circuit. The current source (I_{bias}) and the bias resistor set up a constant voltage across the sensor and the SQUID input coil. Changes in the current through the sensor (tungsten meander) cause a magnetic flux in the coil, which is read by the SQUID.

creases, therefore the current passing through it decreases, and the joule heating decreases. This causes the tungsten meander to bias itself at a temperature in the middle of its superconducting transition. This process is called negative electrothermal feedback because of its parallels to feedback in an op-amp circuit. A positive side effect of ETF-TES is that each individual sensor biases itself at its own T_c . Creating a thin film of tungsten that has a uniform T_c has proven to be difficult but each meander will bias into its own transition. Severe T_c gradients have been measured on detectors from meander to meander, which cause non-uniform event triggers, poor data, and make the detectors difficult to operate, calibrate, and analyze the data from. This motivates the search for a uniform T_c detector.

Phonons are produced in an event in the detector, and this leads to the tungsten meanders to heat up and increase their resistance. Because the TES is voltage biased, this causes a change in the current passing through the tungsten, which is measured by a SQUID (and appropriate SQUID-amp circuitry). See figure 4.

Quantitatively, the TES process can be described as follows. For more detail, see [8, 14]. The power flow equation describes how power flows into and out of a tungsten meander

$$C \frac{dT}{dt} = \frac{V_0^2}{R(T)} - K (T_w^n - T_S^n). \quad (1)$$

See figure 5. Here C is the heat capacity of the tungsten, $\frac{dT}{dt}$ is the change in temperature T with respect to time t , V_0 is the bias voltage, R is the resistance of the meander, K is

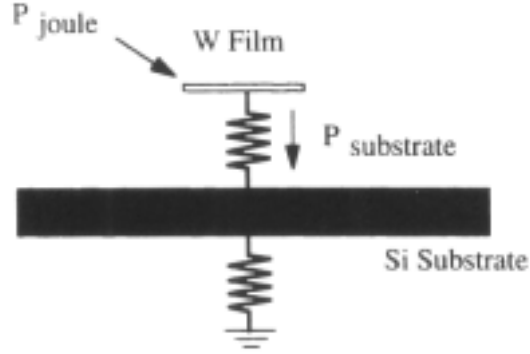


Figure 5: Power flow into (joule heating) and out of (heat flow to the substrate) a tungsten (W) meander on a detector.

a material and geometry dependent constant that characterizes the thermal conductance between the tungsten and the substrate, and T_S is the temperature of the substrate. n can be 4, 5, or 6, depending on thermal impedance between the tungsten and the substrate, and the model used. We use $n = 5$.

Events cause a small change in temperature, so equation 1 can be expanded in ΔT , discarding higher order terms:

$$C \frac{dT}{dt} = -\frac{V^2}{R_0^2} \frac{dR}{dT} \Delta T - g \Delta T. \quad (2)$$

Solving the differential equation, 2, yields a simple exponential with time constant

$$\tau_{eff} = \frac{\tau_0 n}{\alpha}.$$

τ_0 is defined as $\frac{C}{g}$, g is the thermal conductance, and α is defined for

$$\alpha \equiv \frac{dR}{dT} \frac{T_0}{R_0}, \quad (3)$$

where T_0 is the transition temperature (also called T_c) and R_0 is the resistance of the tungsten at T_c . It is important to point out that the above calculations are only valid in the extreme negative feedback (ETF) regime, defined where $T_c \gg T_S$ and $\frac{\alpha}{n} \gg 1$. [9]

Equation 2 describes the pulse shape and height, but is not the only analytic expression of interest. The intrinsic noise of an ETF-TES as a function of film T_c and α is of particular interest. Via Fourier analysis of equation 1, we get [9]

$$\Delta E_{FWHM} = 2.36 \sqrt{4kT_0^2 C \frac{1}{\alpha} \sqrt{\frac{n}{2}}}, \quad (4)$$

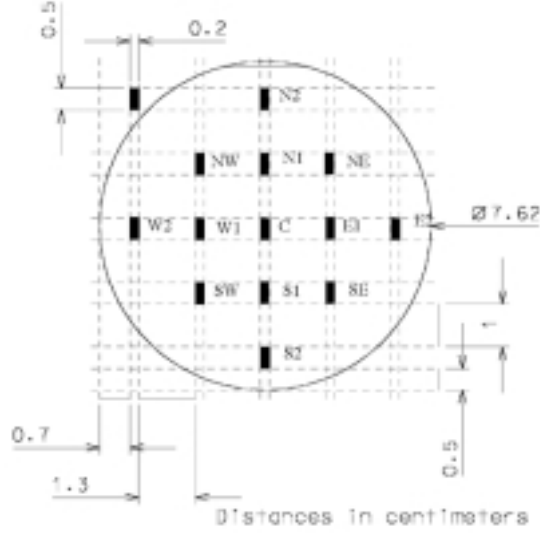


Figure 6: Sample wafer dicing pattern. Samples are labeled with cardinal directions, north at the flat on the wafer.

where ΔE_{FWHM} is the full width-half maximum error in an energy measurement. Since the heat capacity, C , depends on the cube of the temperature,

$$\Delta E_{\text{FWHM}} \propto \sqrt{\frac{T^5}{\alpha}}. \quad (5)$$

From measurements of T_c and α for TES on a detector, the error in energy measured can be calculated.

3 Experimental Setup

3.1 Wafers

Large germanium detectors are expensive and hard to handle, therefore when detectors are sputtered with tungsten, thin silicon wafers are also placed in the sputtering device. This provides us with detectors and matching test wafers which have tungsten properties the same as the detector. Sputtering is done with a Balzers 450 DC-magnetron sputtering system in California by our collaborators. It is these test wafers that are diced up at CWRU, so we can measure T_c at various places on the detector that that wafer corresponds to.

Wafers are diced into a standard thirteen sample pattern as shown in figure 6. This allows us to map and profile any gradient in T_c . A finer sampling of the wafer is not made because of limitations in the number of total samples we can place in the fridge as discussed below.

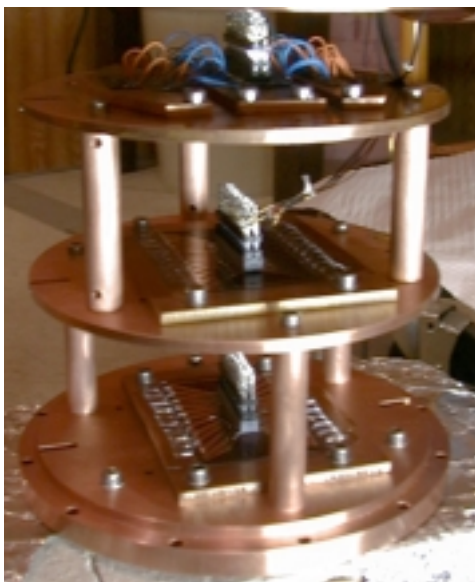


Figure 7: The Mini-Tower ready to be installed in the fridge. The lower two plates hold tungsten samples, the top plate is being used to calibrate RuO_2 thermometers. The outer ring on the lower plate is bolted to the bottom of the mixing chamber of the Oxford fridge.

3.2 Kelvinox

An Oxford Kelvinox-100 helium dilution refrigerator is used to cool the samples to millikelvin temperatures. Samples are mounted with General Electric type 3071 varnish (GE-varnish) to a copper plate. GE-varnish thinned with ethyl alcohol is placed on the copper, and the samples are placed on top. The samples are held in place with small spring loaded clamps, and the plate is baked to cure the varnish. Three plates are bolted to each other with copper risers in a tower-like configuration affectionately named the mini-tower. The mini-tower was designed to keep all layers at the same temperature and is bolted to the mixing chamber (experimental) layer of the fridge. See figure 7.

3.3 Measurement

Resistance measurements are made with a modified 4-wire measurement to conserve wiring. All samples are connected in series, and current biases all samples. Voltage lines are placed in between samples, so that each sample shares lines with its neighbor. Heat-sinking wires to the mixing chamber is difficult, therefore this reduction in required wiring allows us to nearly quadruple the number of samples we can measure. See figure 8.

Samples are wire-bonded with aluminum wire to a home made copper clad Kapton surface. See figure 9. Cryogenic (quad lead) wires are soldered to 24-pin samtec connectors, which connect the copper Kapton with the mixing chamber heat-sink. See figure [plate]. Similar quad lead-samtec cables connect successive heat sinks in the fridge. At the 1.2

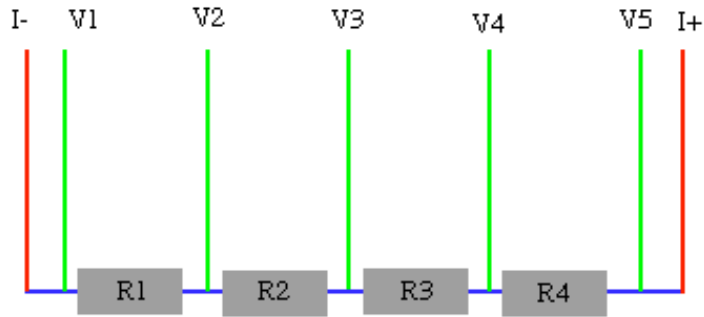


Figure 8: Block diagram of modified 4-wire measurement technique. Grey is tungsten, blue is copper and aluminum wire bonds, red is current leads, and green is voltage leads.

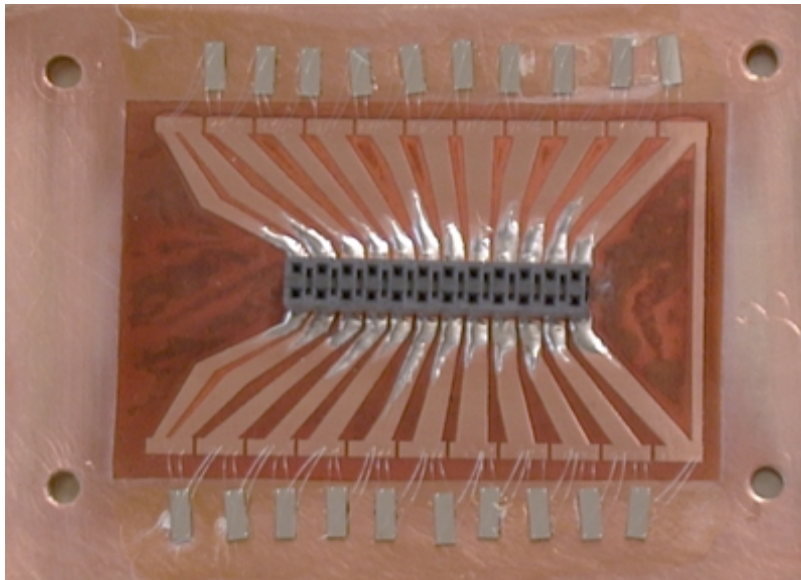


Figure 9: Tungsten samples, mounted and wire-bonded on the copper mounting plate. At the center is the samtec connector, which connects the samples to the outside world.

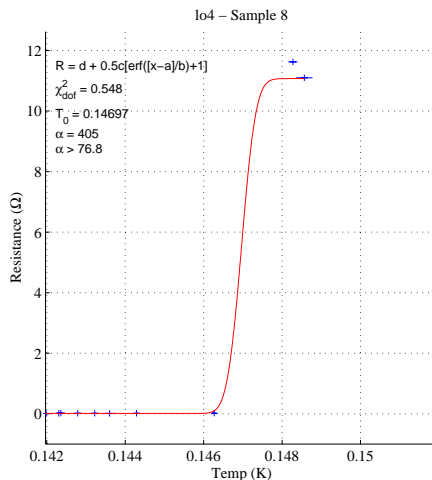


Figure 10: Resistance vs. Temperature for the N2 sample of wafer 99-t-202. The line is the erf fit to data marked with '+'s.

kelvin layer, connections are made to MDM connectors which lead to Fisher-24 connectors at the exterior of the fridge. From the Fishers, home made cables connect to an LR-700 AC resistance bridge with LR-720 multiplexing unit. The LR-700 is connected to a data acquisition computer (DaqMac) via a GPIB bus, and LabView VIs were written that record the data and control the temperature of the fridge allowing for data taking at night when the fridge is running.

4 Data & Results

4.1 T_c Measurements

Samples from four different test wafers was taken in the last fridge run (CWRU Run 6). When taking data, care must be taken not to set the excitation voltage on the LR-700 too high, so as to artificially heat the tungsten samples. Before taking automatic measurements, we manually determine what excitation causes artificial heating in the samples. For the remaining measurements, we set the excitation a few orders of magnitude (if possible) below this threshold. Example data are shown in figures 10 and 11. Figure 10 depicts the more common case where no data points could be taken in the transition, the sample was either superconducting or not. Figure 11 depicts data where transition points were seen.

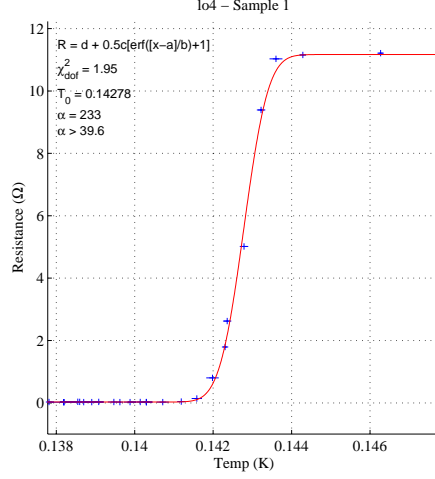


Figure 11: Resistance vs. Temperature for the NE sample of wafer 99-t-198. The line is the erf fit to data marked with ‘+’s.

4.2 Fits

Data from DaqMac was loaded onto a UNIX machine and analyzed with MatLab 5.2.0.3084. Transitions were empirically fit with an error function of the form

$$R = \frac{C}{2} \operatorname{erf} \left(\frac{T - A}{B} + 1 \right) + D, \quad (6)$$

where the error function is defined as

$$\operatorname{erf}(x) \equiv \frac{2}{\sqrt{\pi}} \int_0^x e^{-t^2} dt.$$

The error function is chosen because of its empirical similarity to the shape of the transition and T_c and α are easily extracted from the functional form. From the 4 fit parameters we get

$$\begin{aligned} T_c &= A \\ \alpha &= \frac{2A}{B\sqrt{\pi}} \\ R_{\text{normal}} &= C \\ \text{zero offset} &= D. \end{aligned}$$

R_{normal} depends on the geometry of the tungsten sample, and the zero offset measures the resistance in the small amount of copper and aluminum in the current path between the voltage leads (see figure 8).

4.3 α

With our setup, measuring T_c was simple, measuring α was not. Only one transition had several data points in the transition, others only had normal and superconducting points

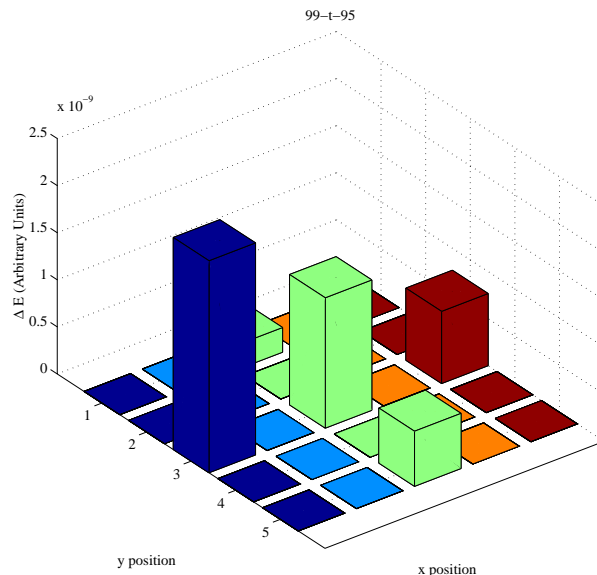


Figure 12: ΔE_{FWHM} vs. position on wafer 99-t-95. The $x - y$ grid is uniformly spaced on the wafers, and points correspond to the cardinal directions on the wafer layout. Points with zero height were not measured.

(see figure 10). Holding the fridge steady at a very precise temperature was difficult, and the finest steps that we could get didn't get many transition points. When no data points in the transition were made, only a lower limit on α can be made. The slope between the warmest superconducting and the coldest normal point is used to calculate the lower limit:

$$\alpha > \left(\frac{\Delta R}{\Delta T} \right) \left(\frac{T_0}{R_0} \right).$$

The expression for the error (equation 5) depends on the inverse square root of α , but depends on the square root of T_c^5 . Therefore α is not as important, and the use of a constant α over the wafers is sufficient. [13] We chose $\alpha = 233$ because it is equal to the precise measurement from the one data set, and agrees with the lower limits from all other data sets. For future work, better determinations of α may prove interesting.

4.4 Results

Several different wafers have been tested at CWRU. Early wafers that were tested (99-t-95, 99-t-147, and 99-t-149) showed large gradients in T_c . This causes a significant gradient in the error for different parts of a corresponding detector. See figures 12, 13, and 14. These earlier wafers were sputtered with low Balzers voltage in an effort to lower the T_c of the tungsten. However with low Balzers voltage, un-predictable gradients and fluctuations in T_c tend to occur.

The wafers produced recently (99-t-194, 99-t-198, and 99-t-202) have a negligible T_c gradient. As is seen in figures 15, 16, and 17, this translates into consistent errors along the

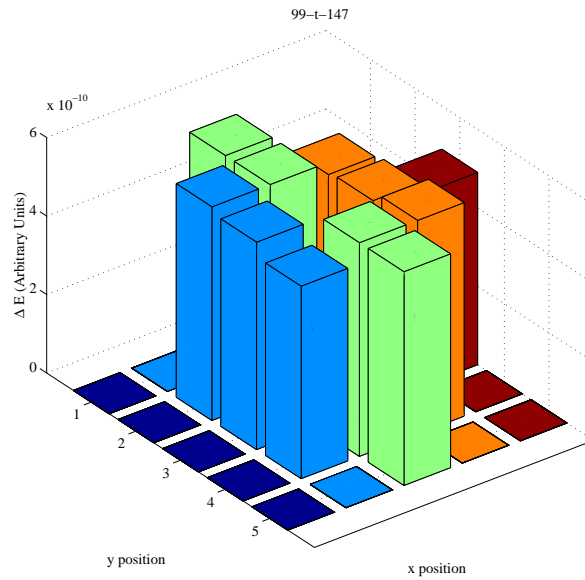


Figure 13: ΔE_{FWHM} vs. position on wafer 99-t-147. The $x - y$ grid is uniformly spaced on the wafers, and points correspond to the cardinal directions on the wafer layout. Points with zero height were not measured.

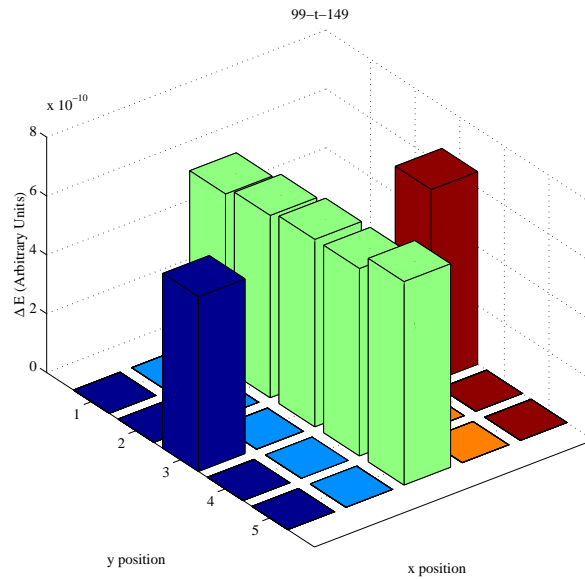


Figure 14: ΔE_{FWHM} vs. position on wafer 99-t-149. The $x - y$ grid is uniformly spaced on the wafers, and points correspond to the cardinal directions on the wafer layout. Points with zero height were not measured.

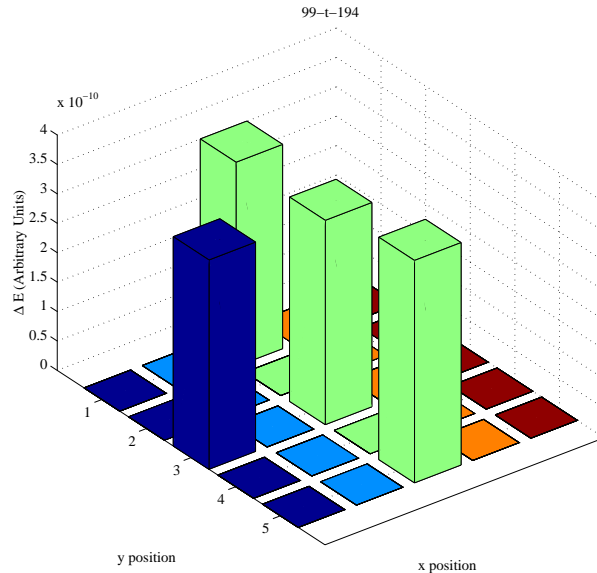


Figure 15: ΔE_{FWHM} vs. position on wafer 99-t-194. The $x - y$ grid is uniformly spaced on the wafers, and points correspond to the cardinal directions on the wafer layout. Points with zero height were not measured.

wafer, and therefore along a detector. Cleanliness of the Balzers has helped stabilized T_c , along with an increased Balzers voltage at the price of higher overall T_c values.

5 Conclusion

CDMS is a large collaboration, searching for WIMP dark matter. CDMS detectors utilize tungsten ETF-TES to measure the energy of phonons, and the error in this energy measurement depends on the superconducting transition temperature of the tungsten. The original wafers and detectors had a significant gradient in T_c , and therefore a large gradient in the error. More recent wafers have a much smaller T_c gradient at the cost of a higher (less preferable) T_c .

A new technique that allows for the uniform tuning (lowering) of T_c on a wafer after sputtering has just been developed by members of the collaboration. [4] Iron ions are implanted in the tungsten in precise concentrations. This will allow for appropriately low T_c wafers because of implantation, but appropriately small T_c fluctuations because of the improved Balzers technique.

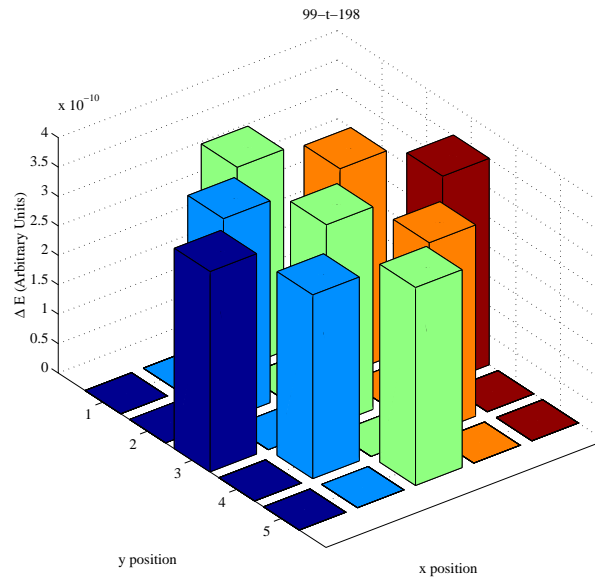


Figure 16: ΔE_{FWHM} vs. position on wafer 99-t-198. The $x - y$ grid is uniformly spaced on the wafers, and points correspond to the cardinal directions on the wafer layout. Points with zero height were not measured.

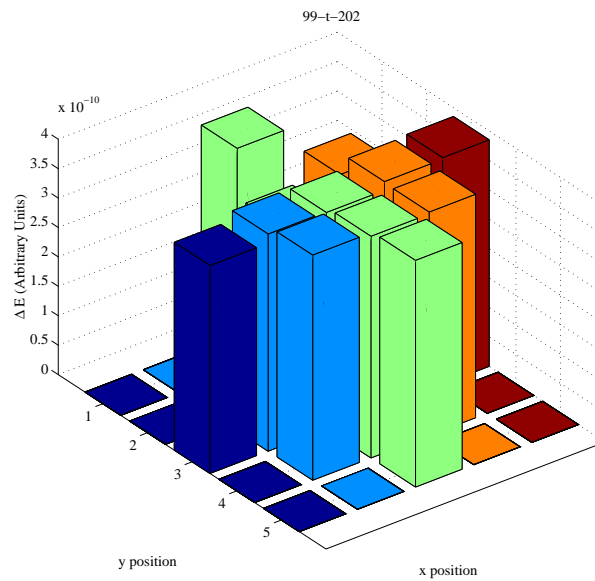


Figure 17: ΔE_{FWHM} vs. position on wafer 99-t-202. The $x - y$ grid is uniformly spaced on the wafers, and points correspond to the cardinal directions on the wafer layout. Points with zero height were not measured.

6 Acknowledgements

First I would like to thank Kent David Irwin and Sae Woo Nam, whose PhD thesis were very helpful, and who unknowingly provided me with figures 1, 3, 2, 4, and 5 so I would have time to finish writing not 5 minutes before this thesis was due.

Thanks to Alex Bolozdynya, Thushara Perera, Donald Driscoll, Moshe Katz-Hyman, Timothy Peshek, Gensheng Wang, Natalie Schommer, Peter Hyland, and Cheshana Marshall. These are the people who ran the fridge, wired the fridge, made things work, and made the lab run. Without them, I couldn't have done anything, from understanding physics to data to analysis (MatLab!), and Beer Day!

I have to thank all my friends who have entertained me (and pulled me away from work) during the past few weeks, specifically the 2000 SpringFest PAC Liquid Nitrogen Ice Cream #1 Award Winning Booth crew, the crazy PAC people at the BBQ, my Commuter Contemporaries, and all purveyors of REEB everywhere!

Finally I would like to thank my thesis advisor, Prof. Dan Akerib. The man who has been my mentor, teacher, advisor, professor, and friend for my last two years at CWRU. As his first undergraduate 'advisee,' I can only envy his future students who will have such an intelligent, fun, and caring advisor to give them the best conclusion to their CWRU careers possible. Take care, skipper!

References

- [1] D. S. Akerib. Personal communications. 2000.
- [2] J. Binney and S. Tremaine. *Galactic Dynamics*. Princeton University Press, 1987.
- [3] N. E. Booth. *Applied Physics Letters*, 50(293), 1987.
- [4] B. A. Young et. al. Measurement of t_c suppression in tungsten using magnetic impurities. *Journal of Applied Physics*, 86(12), 1999.
- [5] M. Zeilik et. al. *Introductory Astronomy and Astrophysics*. Saunders College Publishing, 1992.
- [6] M. W. Goodman and E. Witten. Detectability of certain dark-matter candidates. *Physical Review*, D31(12), 1985.
- [7] G. Jungman M. Kamionkowski K. Griest. Supersymmetric dark matter. *Physics Reports*, 1995.
- [8] K. D. Irwin. An application of electrothermal feedback for high resolution cryogenic particle detection. *Applied Physics Letters*, 66(15), 1998.
- [9] Kent David Irwin. *Phonon-Mediated Particle Detection Using Superconducting Tungsten Transition-Edge Sensors*. PhD thesis, Stanford University, 1995.
- [10] M. Kamionkowski. Wimp and axion dark matter. In *1997 ICTP Summer School on High Energy Physics and Cosmology*, 1997.
- [11] B. W. Lee and S. Weinberg. Cosmological lower bound on heavy-neutrino masses. *Physical Review Letters*, 39(4), 1977.
- [12] J. D. Lewin and P. F. Smith. Review of mathematics, numerical factors, and corrections for dark matter experiments based on elastic nuclear recoil. *Unknown Journal*, 1996.
- [13] S. W. Nam and B. Cabrera. Personal communications. 2000.
- [14] Sae Woo Nam. *Development of Phonon-Mediated Cryogenic Particle Detectors With Electron and Nuclear Recoil Discrimination*. PhD thesis, Stanford University, 1998.
- [15] J. A. Peacock. *Cosmological Physics*. Cambridge University Press, 1990.
- [16] T. A. Perera. Personal communications. 2000.
- [17] M. S. Turner. Cosmological parameters. *astro-ph/9904051*, 1999.